Optics & Laser Technology 193 (2026) 114233

Contents lists available at ScienceDirect

Optics and Laser Technology

journal homepage: www.elsevier.com/locate/optlastec

Full length article

Gain-managed nonlinear amplification and noise performance of an Yb-doped fiber amplifier seeded at different wavelengths

Sara Pizzurro [a], Riccardo Gotti [a,*], Xhoi Ypi [a], Francesco Canella [b], Dario Giannotti [c], Gianluca Galzerano [b], Antonio Agnesi [a], Federico Pirzio [a]

[a] Dipartimento di Ingegneria Industriale e dell'Informazione, Via Ferrata 5, Pavia 27100, Italy
[b] Istituto di Fotonica e Nanotecnologie, Consiglio Nazionale delle Ricerche, Piazza Leonardo da Vinci 32, Milano 20133, Italy
[c] Dipartimento di Fisica, Politecnico di Milano, Piazza Leonardo da Vinci 32, Milano 20133, Italy

ARTICLE INFO

Keywords:
Fiber lasers
Fiber amplifiers
Ultrafast lasers
Mode-locked lasers
Lasers noise

ABSTRACT

The performance of a low-noise, Yb-doped nonlinear fiber amplifier seeded by a spectrally-filtered ~8-MHz ultrafast fiber Mamyshev oscillator was investigated across input wavelengths from ~1040 to 1064 nm. Using a simple and efficient setup, pulses as short as 31 fs with a small pedestal and energy up to 120 nJ were achieved from <1 nJ input pulses at shorter wavelengths. A detailed characterization of the noise performance of the master oscillator and the gain-managed nonlinear amplifier showed a relative intensity noise at a level of 0.2 % in the integration bandwidth from 2 Hz up to half of the repetition rate, highlighting the exceptional stability of the system.

1. Introduction

Amplification of ultrashort pulses in fiber amplifiers is attractive for many applications requiring significantly higher energy than usually available from conventional ultrafast fiber lasers [1–3]. Chirped-pulse amplification (CPA) [4] allows the most flexible solution since the seed pulse can be conveniently stretched to maintain a safe peak power level at any repetition rate and average output power. However, the post-compression pulse duration is basically limited by the gain narrowing due to the finite fiber amplifier bandwidth [2]. A recently identified pulse-propagation regime, called gain-managed nonlinear amplification (GMNA) [5], exploits a particular spectral shaping in Yb-doped fiber amplifiers. Owing to the interplay of positive dispersion and spectral gain evolution with pulse amplification along the fiber, the typically sub-picosecond seed pulse is amplified reaching a spectral width exceeding the gain bandwidth of the amplifier itself. Such spectral width can be as broad as ~100 nm and extends from the absorption edge of the quasi-three level Yb amplifier up to the Raman resonance that tends eventually to degrade the pulse quality, adding incoherent contributions [6]. The resulting amplified pulse is typically a few picoseconds long, with monotonic chirp, its energy being limited by the onset of stimulated Raman scattering (SRS) and ultimately related to the fiber core area. Therefore, GMNA allows in principle to reach superior performance in terms of short pulses of high quality (low pedestal), although with a pulse energy that is strictly limited by the fiber core size, regardless of the repetition rate. For comparison, a CPA amplifier with a fixed pump power can be designed for output pulses of higher energy by reducing the pulse repetition rate and adjusting the pulse pre-stretching. GMNA has been extensively investigated numerically and experimentally [5,7,8], although always with seed pulses at wavelengths close to the Yb-ion gain peak, around 1030 nm. More recently, GMNA has also been demonstrated in an Er-doped fiber system seeded at 1530 and 1560 nm [9]. In that work, it was shown that the choice of the seeding wavelength close to the short-wavelength edge of the gain spectrum is less critical to reach the GMNA regime compared to Yb-doped fiber systems such as the one investigated here.

In this work, we employed a tunable ultrafast low-power Mamyshev fiber oscillator (MO) to cover the 1040–1064 nm extended range of practical interest for GMNA, enabling an investigation into the amplifier's performance, focusing on post-compression pulse duration, pulse energy, pedestal amplitude, and energy. For our experimental study, it is not strictly necessary to use a filtered Mamyshev oscillator as the seed; any mode-locked laser providing experimental parameters comparable to those reported in the Amplification Results section would be suitable. A study in the wavelength range close to the gain peak of the Yb amplifier was previously reported by Ye et al. [10], with qualitatively

* Corresponding author.
E-mail address: riccardo.gotti@unipv.it (R. Gotti).

https://doi.org/10.1016/j.optlastec.2025.114233
Received 17 September 2025; Received in revised form 14 October 2025; Accepted 30 October 2025
Available online 13 November 2025

similar results, although not reaching the limit of short pulse generation from the GMNA due to the ~4-time lower final pulse energy in the same type of Yb-fiber amplifier. We also investigated the possible contribution of amplified spontaneous emission (ASE), given the low level of injected average power in our setup. However, this turned out to be only a few percent of the total output power, therefore perfectly acceptable for many applications that rely on frequency up- or down-conversion of the fundamental pulse train, where the nonlinear process efficiently suppresses the low-intensity ASE noise. We also carried out a detailed characterization of the relative intensity noise (RIN) performance of both the seeder and the amplified pulse train. Our results well compare to those previously reported in [11,12]. In particular, the values of the RIN power spectral density (at −120 dB/Hz for Fourier frequencies above 10 kHz) are comparable to those reported for a similar MO generating a pulse train at 7.6 MHz with average powers between 30 and 130 mW [11]. Notably, in our amplified system, the same RIN values—resulting in an integrated intensity noise of 0.2 % within a 2 Hz to 4.15 MHz bandwidth ($f_{rep}/2$)—are achieved at higher average powers of up to 1 W and compressed pulse durations of 31 fs. Furthermore, the long-term stability of the pulse energy surpasses that reported in [11], achieving a remarkable 0.2 % stability over an observation period of one hour. The pulse repetition frequency jitter was also analyzed with a minimum sensitivity of 8 fs^2/Hz, resulting in a root mean square value of 14 ps for the amplified pulse train within the integration bandwidth of 100 Hz to 4 MHz. The excellent pulse quality, very high peak power even at a relatively low average power level, and the low intensity noise performance make this robust and compact fiber laser system very promising for nonlinear optics applications such as mid-IR frequency down-conversion or THz generation.

2. Amplification Experiments

We set up an ultrafast MO, started by a microchip passively Q-switched (PQS) laser like the one described in Ref. [13]. The ~20-nm wide output spectrum of the low-power oscillator is centered either at 1035 nm (see Fig. 1, inset "a") or at 1064 nm, depending on the chosen wavelength of the PQS laser used for starting the MO, as it is described in Ref. [14]. The seeder MO has an average power of about 30 mW with a pulse repetition rate of ~8.3 MHz. The output chirped pulse of the MO is typically few picosecond long and can be compressed to ~100 fs duration. However, for the GMNA investigation work we used a flat-top hard-edge commercial passband filter (BPF, model Semrock MaxLine LL01-1064–12.5) to sample three specific wavelengths in the target range. The filter has a ~3-nm wide transmission window centered at 1064 nm at normal incidence. Within this relatively narrow spectral window (if compared to the full spectrum of the seeder pulses), the spectral phase is almost constant, leading to close to Fourier-Transform limited ~700 fs pulses. Moreover, the transmitted central output wavelength can be blue-shifted of a few nm by tilting the filter. In this way, we tested the fiber amplifier in the GMNA regime by injecting three different wavelengths: 1042 nm, 1052 nm and 1064 nm. In principle, even a seed wavelength as short as 1020 nm would be possible given the MO spectrum in Fig. 1a. However, below 1030 nm the available power after the BPF drops significantly. Furthermore, spectral fringes in the range 1030–1035 nm (possibly due to small satellite pulses in the MO) increase the noise of the nonlinear amplifier significantly when seeded in this range, owing to competition for gain and nonlinear effects. Although the results are very similar to those obtained at ~1040 nm, we decided not to include them in this report due to their inferior noise properties. As already noted in the Introduction, any mode-locked laser providing comparable average power, repetition rate, pulse energy, and duration to those reported here could serve as a suitable seed for achieving similar experimental results.

As it is shown in Fig. 1, a Faraday isolator (FI) was placed after the MO to protect the oscillator from back reflections coming from the fiber amplifier. The average power of the seed pulses after the FI and BPF (see Fig. 1b) was about 2.5 mW. The amplifier consists of a 3.8-m-long, Yb-doped, polarization maintaining, double-clad fiber with a nominal mode-field diameter of 11 μm (Thorlabs YB1200-10/125DC-PM). The active fiber was angle cleaved at both edges to prevent self-oscillation and was pumped with a 7-W multimode fiber coupled laser diode at 976 nm in a co-propagating configuration. After the fiber amplifier, we placed a second FI before the compression stage. The compressor was realized with two transmission gratings (1000 grooves/mm, design wavelength 1040 nm, single pass transmission >97 %) in the Treacy configuration [15]. The total transmission of the FI and the compressor was about 80 %. All the average power measurements we report were performed after the compressor. As it is shown in Fig. 1, the output beam

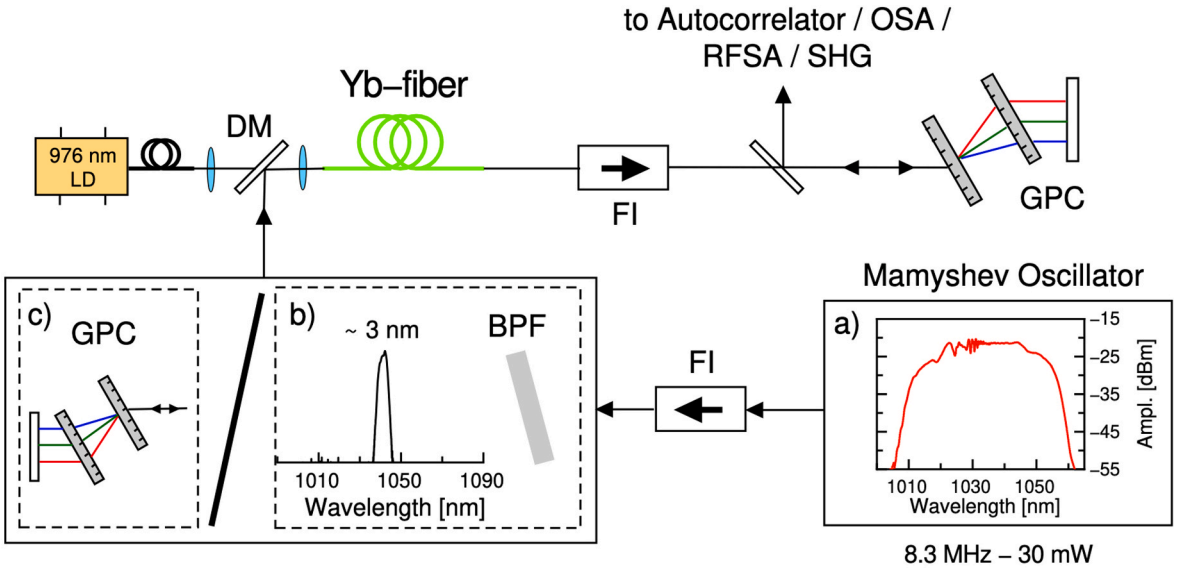

Fig. 1. Ultrafast fiber Master Oscillator Power Amplifier laser system setup. FI: Faraday Isolator; GPC: Grating Pulse Compressor; BPF: dielectric band-pass transmission filter; LD: multimode (NA = 0.22, fiber diameter 100 μm) fiber coupled laser diode at 976 nm; DM: dichroic mirror highly reflective at 1000–1100 nm and highly transmitting at 976 nm; Yb-fiber: polarization-maintaining Yb-doped fiber. Insets: a) typical optical spectrum of the MO when the PQS starter wavelength was 1035 nm; b) angle-tuned BPF to select a ~3-nm wide portion of the MO spectrum to seed the amplifier; c) a GPC to compress the pulses out of the MO and adjust the pre-chirp before seeding the amplifier with the full MO spectrum.

was directed to one of several instruments: a commercial autocorrelator (model A.P.E. pulseCheck-50-NX), an optical spectrum analyzer (OSA, Yokogawa ANDO AQ6317B), a radio-frequency spectrum analyzer (RFSA, Agilent PSA E4445A) or to the Second-Harmonic Generation (SHG) stage, to fully characterize the amplified pulse train in terms of compressed pulse duration, optical spectrum, relative intensity noise (RIN) and residual pedestal/ASE background.

Fig. 2 shows the recorded fiber amplifier output spectra at the maximum diode pump power for each of the three seeding wavelengths. The comparison reveals that as the seed wavelength decreased from 1064 nm to ~1040 nm, the amplified spectrum became markedly non-symmetrical, exhibiting a steep edge on the blue side (see Fig. 2c), where the absorption edge of the Yb-doped amplifier below 1 μm was reached. This behavior is typical when the GMNA regime is achieved [5]. This is in stark contrast with the behavior of the amplifier when seeded at 1064 nm (Fig. 2a) which exhibits an almost spectrally symmetric broadening, with the characteristic features of self-phase modulation and wave-breaking at the two sides. This indicates that the GMNA regime has not been fully achieved for this injected wavelength at the maximum pump power investigated here of 6 W. Even though the two spectral sides appear nearly symmetrical, the region around 1150 nm already exhibits SRS. In fact, further increasing the pump power only enhances this contribution. This effect is more clearly visible in the second-harmonic AC traces (see discussion below), where the SRS manifests as a pedestal, which worsens with increasing pump power if the GMNA regime is not reached. As in Ref. [16], we observed some fringes in the blue side of the spectrum that arise from the interference of the main pulse with a small, delayed satellite that we could notice in a long-scan autocorrelation (AC) trace at a distance of about 4 ps from the main pulse and with a relative amplitude lower than 0.5 % of the main AC trace peak. Fig. 3 shows the non-collinear second harmonic AC trace of the pulses after compression for the three different seeder wavelengths

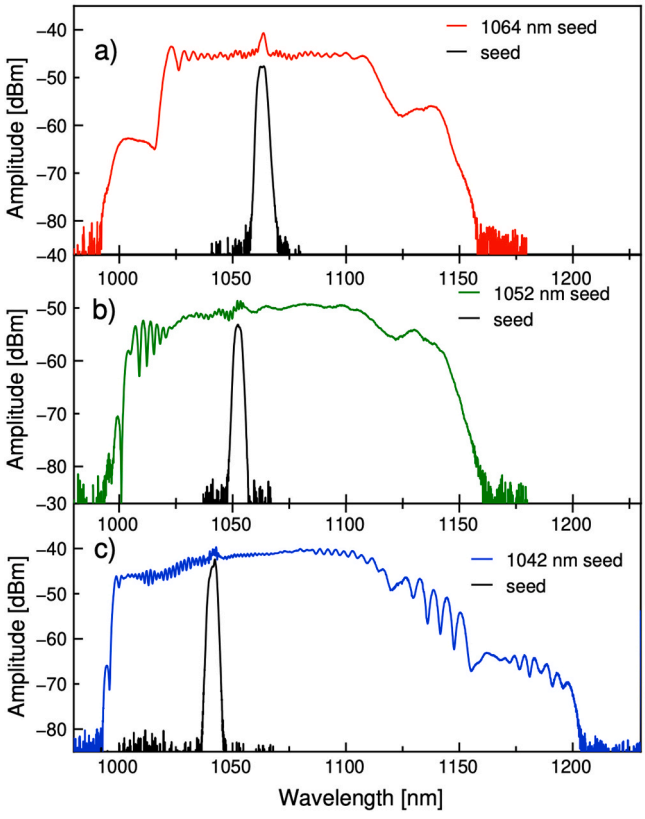

Fig. 2. Amplified spectra at different seeder wavelengths at the maximum pump power.

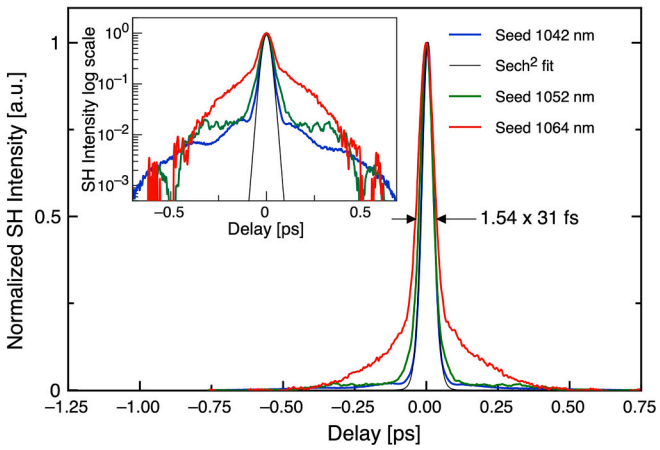

Fig. 3. AC traces of the amplified pulses for the three different seeding wavelengths in linear vertical scale (normalized to the peak value). In black it is shown the best fit with sech^2 autocorrelation function for the shortest pulse achieved seeding at 1042 nm. In the inset it is shown the logarithmic vertical axis representation.

at the maximum pump power, as measured with a commercial autocorrelator. The log-scale representation (inset of Fig. 3) emphasizes the pedestal in the AC traces, enhancing the understanding of the drastic improvement in pulse quality after compression that we observed as the seeder wavelength was changed from 1064 nm to 1042 nm. In addition to the better pulse quality, the blue shift of the seeding wavelength leads to a significant reduction of the compressed minimum pulse duration from about 50 fs for 1064 nm seeding to 31 fs when seeding at 1042 nm.

A further proof of the full evolution towards GMNA regime when seeding at shorter wavelength can be obtained analyzing the amplified pulses spectra at the seeder wavelength of 1042 nm at different pump power level (see Fig. 4). At the beginning of the amplification process (P_{pump} ~2 W) the spectrum exhibits nearly symmetrical broadening, extending over 60 nm. This also occurs for the other injected wavelengths; however, by increasing the pump power the GMNA regime is fully reached only for the shorter ones, before SRS sets in and destabilizes the pulse train. At this pump level, the pulse energy after compression is about 30 nJ. As the pump power increases to ~4 W (green curve in Fig. 4), the spectral broadening starts to be nonsymmetrical as the blue side gets closer to the re-absorption edge of the Yb-doped fiber. Eventually, at the maximum injected pump power of 6 W, the blue side of the spectrum has reached the ~1 μm edge and the red-side is extending well above the gain bandwidth of Yb-fiber, up to 1200 nm. At this pump power level, SRS began to appear in the spectrum, though it did not yet significantly affected the compressed pulse quality. As the pump power is further increased, a few ps-long pedestal appears in the AC trace, clearly indicating that incoherent contributions due to SRS start degrading the pulse quality.

In Fig. 5 we report the output power/energy characteristics for the three selected seeder wavelengths as a function of the diode pump power. The maximum pump power level was chosen for each measurement when the SRS contribution started to be evident in the amplified pulse spectrum and AC traces. As expected from the shape of the emission cross section of the Yb-doped amplifier, seeding at shorter wavelengths helps improve the amplifier performance. The long-term average power stability measurement of the amplified signal injected at 1042 nm is shown in the inset in Fig. 5. The power was recorded after the compressor at the maximum pump power level over a one-hour run. The results demonstrate an excellent stability of the average output power with fluctuations of only ~0.18 % rms.

Given the relatively low average power of the injected seed, we decided to assess the amount of ASE background in the average power measured after amplification. Given the very wide bandwidth of the

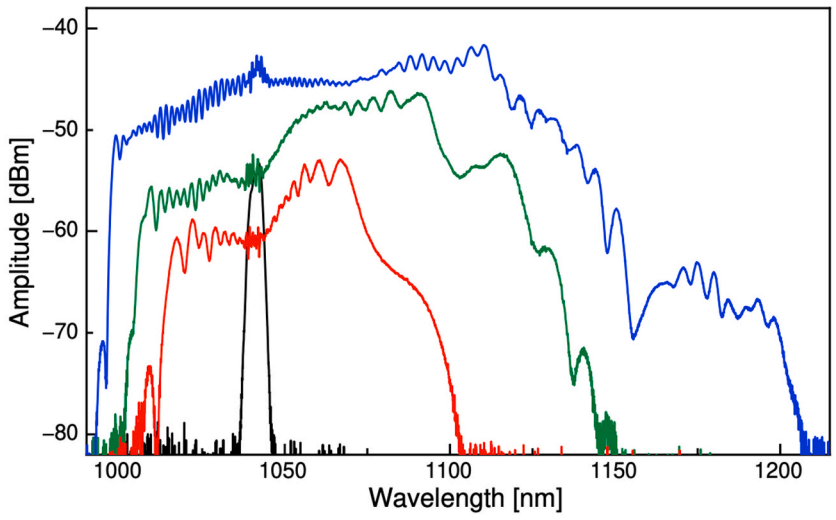

Fig. 4. Evolution of the amplified spectra at the seeder wavelength of 1042 nm (black curve) at different diode pump power: the red curve represents the spectrum when we inject a pump power of 2.3 W, the green curve at 4.2 W and the blue curve at the maximum pump power of 6 W.

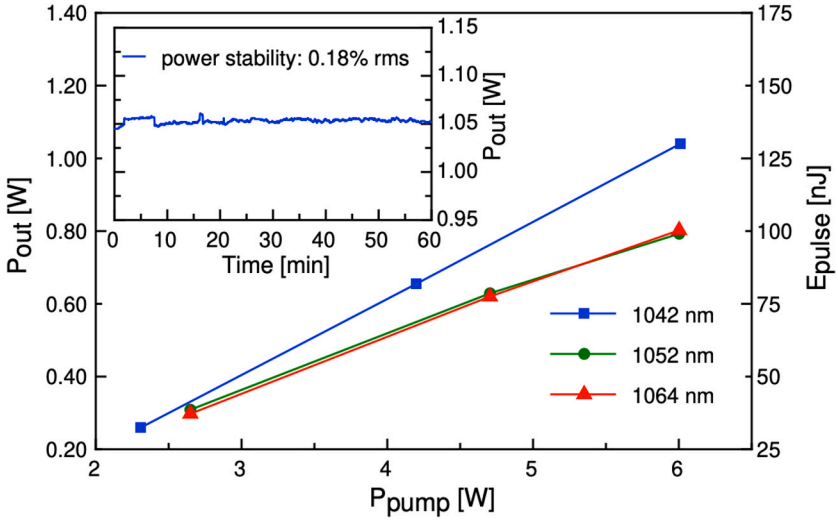

Fig. 5. Average output power and pulse energy as a function of the diode pump power for seeding wavelengths of 1042 nm (blue), 1052 nm (green) and 1064 nm (red). The inset shows the average power stability of the amplified signal seeded at 1042 nm registered at the maximum pump power over one hour.

amplified pulses, we could not determine any ASE contribution by directly observing the output spectrum. Alternatively, in the literature, methods have been reported to evaluate the ASE contribution, e.g., by synchronizing the deflection window of an acousto-optic modulator with the pulse train, and measuring the residual signal between pulses as arising from ASE [18]. Here instead, we propose a different and simpler approach, which permits to determine the ASE background when it is larger than few percent of the average output power. We set up a SHG stage employing an achromatic half-wave plate and a 3-mm-long Type I LBO crystal. We used either a Schott BG38 or OG-590 filter to alternately suppress the fundamental or SHG beam, respectively. By adjusting the half-wave plate, SHG can be maximized or extinguished. In this way, we recorded on the oscilloscope the undepleted and depleted laser pulses of the fundamental beam by means of a sub-nanosecond InGaAs photodiode. This provides a direct indication of the effective pulse-to-pulse SHG conversion efficiency. In the meantime, the SHG average power alone can be simply measured by means of a power meter once the fundamental beam has been filtered out. By comparing the single pulse conversion efficiency and the conversion efficiency measured on the pulse train average power (which is lower due to the low-intensity, unconverted noise background), one can infer the ASE content in the average power measured with the power meter before the SHG stage. For the evaluation of the single-pulse SHG efficiency, statistics over several pulses are required to account for pulse-to-pulse fluctuations. In contrast, the SHG average power is obtained by averaging over multiple measurements The results of the investigation for the different seeder wavelengths are summarized in Table 1, and show that only when seeding at 1064 nm, the ASE background exceeds 10 % of the measured

Table 1
Summary of the main properties of the amplified pulse train as a function of the seeding wavelength.

Seeding wavelength [nm]	1042	1052	1064
Total average output power [W]	1.06	0.78	0.78
ASE contribution	7 %	9.5 %	15 %
Pulse train average output power [W]	0.99	0.7	0.66
Pulse energy [nJ]	120	85	80
Compressed pulse duration [fs]	31	37	50
Pulses peak power [MW]	3.9	2.3	1.6
Area % of the main AC peak	86	83	55

average power. At the best seeding wavelength of 1042 nm, the ASE background is 7 %, less than one half compared to the 1064-nm seeding owing to higher gain and improved saturation of the Yb-fiber amplifier. In Table 1, we also report an estimation of the percentage of energy in the main peak of the AC traces of the compressed pulses as calculated by comparing the area underneath the AC trace with the area underneath the sech^2 best fit of the main lobe of the AC trace. Along with ASE measurement, this yields an accurate estimate of the pulse peak power.

The result of a SHG-FROG measurement (available as an option for our autocorrelator) carried out on the pulses when seeding at 1042 nm at 6 W incident pump power is reported in Fig. 6. The retrieved pulse spectrum (see Fig. 6c) is in reasonable agreement with the measured spectrum and shows a spectral phase almost flat across 1000–1100 nm. The retrieved pulse (see Fig. 6d) presents very small satellites accounting for about only 2 % of the total pulse energy from numerical integration.

The amplifier could be also seeded with the full energy of the oscillator pulse using a pre-compressor to attain the shortest possible pulse duration like in Ref. [7], without any spectral filtering (see Fig. 1). Although pulses as short as 27 fs could be obtained in this manner after the amplifier (see Fig. 7), we found that very critical adjustment of the pulse pre-compressor (corresponding to slightly negative chirp like in Ref. [17]) was required. This might be due to the shorter pulses in our case (~100 fs vs. 230–270 fs [7]) and due to the peculiar spectral shape of the MO. Furthermore, the pedestal contribution was more significant in this case, probably due to the broader spectrum extending beyond the Raman resonance. Besides providing wellseparated single spectral portions for our task, spectral filtering turned out to greatly simplify the seeding of the GMNA, with no need of pre-compression at all, despite the significantly reduced injected energy. Eventually, our seeding parameters closely resembled those reported in Ref. [8]. Indeed, in such conditions, one major concern was the possible contribution of ASE, which

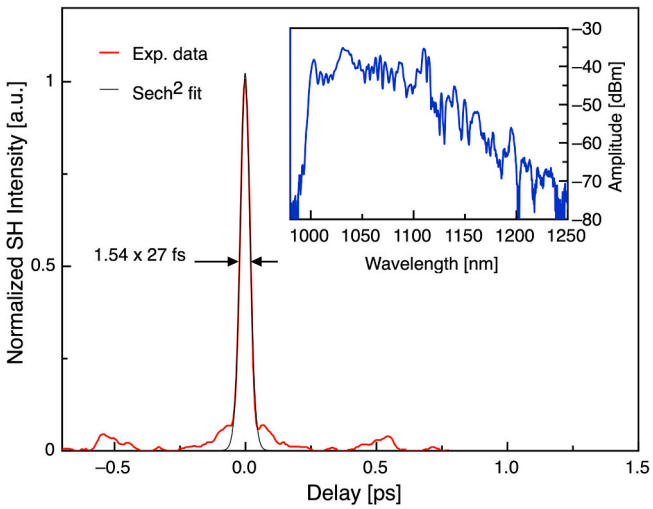

Fig. 7. AC trace of the compressed pulse, normalized to the peak value, obtained seeding the GMNA fiber amplifier with the full energy of the MO and a pre-compressor (see Fig. 1) and sech^2 autocorrelation fit function. In the inset it is shown the corresponding optical spectrum in logarithmic vertical axis scale.

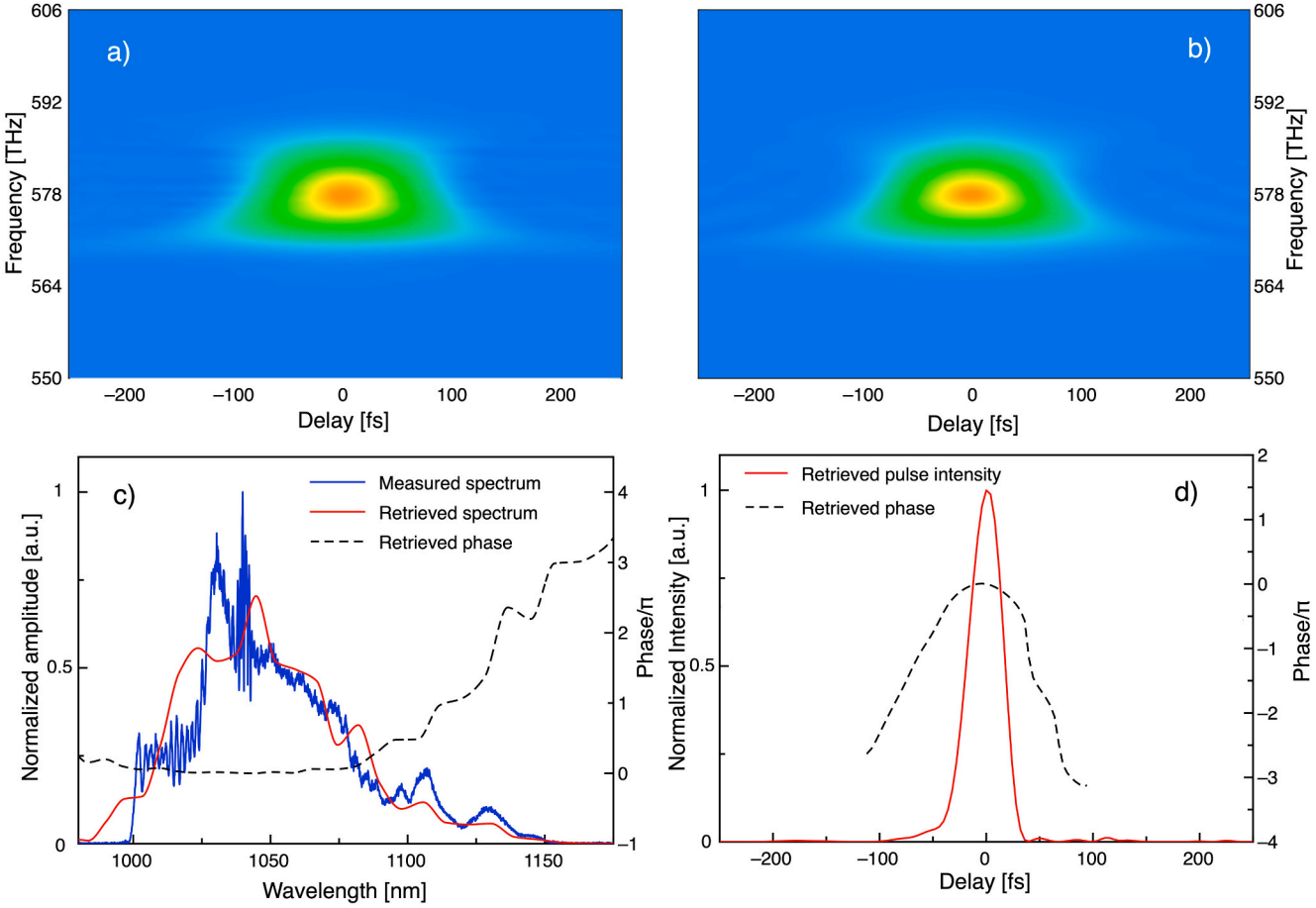

Fig. 6. (a) Measured SHG-FROG trace. (b) Retrieved SHG-FROG trace with 0.0073 error on a 128 × 128 grid. (c) Pulse optical spectrum (blue line) and retrieved optical spectrum (red line) normalized to the peak value. The retrieved spectral phase in units of π is shown in black dashed line. (d) Retrieved pulse temporal intensity profile, normalized to peak value, and temporal phase in units of π.

was not investigated in previous work. However, this amounted to only a few percent of the total output power in the best case, making it perfectly acceptable for many applications. Reduction of ASE could be achieved in several straightforward ways. One could provide pre-amplification of the narrow-band seed, for a more uniform saturation of the amplifier. A seed MO with a noise-free spectrum near 1030 nm would access the highest gain possible in the amplifier, helping with saturation and favoring the GMNA regime [10]. It is also expected that ASE would be reduced significantly using a seeder at a higher repetition rate (few tens MHz), hence higher average power like in [7].

3. Characterization of the noise performance

Fig. 8 shows the power spectral densities of the RIN of both the MO seeder and the amplifier, together with the integrated relative noise. The reported RIN are integrated only over the detection bandwidth (2 Hz–4.15 MHz), which quantifies the intensity fluctuations observable with our measurement chain and is the bandwidth-limited approach used in [11]. We are not addressing pulse-to-pulse RIN, because the targeted nonlinear conversions and downstream detectors integrate over many pulses and, therefore, performance is governed by the detection-band RIN rather than single-pulse statistics.

We measured the RIN using a wide bandwidth InGaAs photodetector and an Agilent E4445A electrical spectrum analyzer. The RIN background coincides with the photodiode noise floor. Concerning the curves behavior, we observe a decreasing (f^{-2} and f^{-1}) trend between 2 Hz and an approximately corner frequency of 10 kHz, for both the MO and the amplifier starting with a RIN level around −70 dB/Hz at 2 Hz. The minimum value of the laser RIN is below −130 dB/Hz, while the amplifier RIN exhibits a nearly white power spectral density at high frequencies, with a minimum value of −120 dB/Hz. We attribute this white noise contribution to the amplified spontaneous emission. Several noise peaks are noticeable in the amplifier's spectrum between 100 Hz and 3 kHz ascribed to the amplifier pump diode's electrical noise, which is directly transferred to the amplified signal. The right axis of the diagram in Fig. 8 shows the integrated relative noise, with an integration range between $f_{rep}/2$ and 2 Hz. The high-frequency noise causes the main difference between the integrated noise of the MO seeder and the amplifier, while below 1 MHz, the integrated values have similar behavior. The total integrated relative intensity noises are 0.13 % and 0.21 % for the MO and the amplifier, respectively. We also characterized the phase noise of the system and measured the associated temporal jitter of the generated pulse train. Exploiting the same detector and spectrum analyzer of the RIN measurement, we acquired the two-sided Power Spectral Density (PSD) of the phase noise at around the 12th harmonic of the repetition rate (99.6 MHz) between 10 Hz and $f_{rep}/2$. We measure the noise of the 12th harmonic to increase the phase noise sensitivity with respect to the RIN and to the spectrum analyzer noise floor. Due to the operation of the spectrum analyzer's phase noise function, the spectrum below 10 Hz is meaningless and is omitted from the plots and calculations. By properly integrating the phase noise PSD and after some simple algebra, it is possible to retrieve the pulse jitter. The phase noise spectrum and the jitter are shown for both the MO seeder and the amplifier in Fig. 9, the left and right vertical axes, respectively.

The MO seeder phase noise spectrum stays between −60 dBc/Hz and −80 dBc/Hz below 100 Hz, then it shows a decreasing trend of approximately −30 dB per decade up to 10 kHz, where the phase noise level stabilizes at about −120 dBc/Hz, corresponding to a jitter noise level of 8 fs^2/Hz. A similar behavior can be found for the amplifier phase noise, even though the downward trend begins at 10 Hz and the plateau at high frequencies stabilizes at −110 dBc/Hz. As for the RIN, the amplifier's trace has relevant peaks related to the electrical noise of the pump diode. The temporal jitter has been calculated in the interval 10 Hz – $f_{rep}/2$. In the full bandwidth interval, the MO has 4 times less jitter compared to that of the amplifier, with values of 10.5 ps and 40.1 ps, respectively. For both cases, a significant contribution arises from the very low frequencies (<50 Hz). The integrated jitter from 100 Hz to $f_{rep}/2$ is significantly lower: for the MO 7.7 ps and 14.1 ps for the amplifier.

4. Conclusion

In conclusion, we presented a Yb-fiber GMNA seeded by a Mamyshev oscillator. We investigated the performance of the amplifier in terms of pulse, energy, compressed pulse duration, pulse quality and ASE contribution as a function of the seeding wavelength in the range ~1040–1064 nm. We showed that seeding closer to the peak of the gain of Yb-doped fiber is beneficial to fully reach the GMNA regime, resulting in a higher amplified pulse energy, shorter pulse duration and significantly improved pulse quality (reduction of the pedestal) after compression. Almost pedestal-free, 31-fs, 120-nJ pulses after compression (~4 MW peak power) were obtained when seeding at 1042 nm with only 0.3-nJ, 700-fs pulses at 8.3 MHz repetition rate. For comparison, when seeding with similar pulse energy/duration at 1064 nm, only 80 nJ pulse energy with 50-fs compressed pulse duration was obtained, with a significant pedestal in the AC trace and more than doubled (from 7 % to 15 %) estimated ASE background.

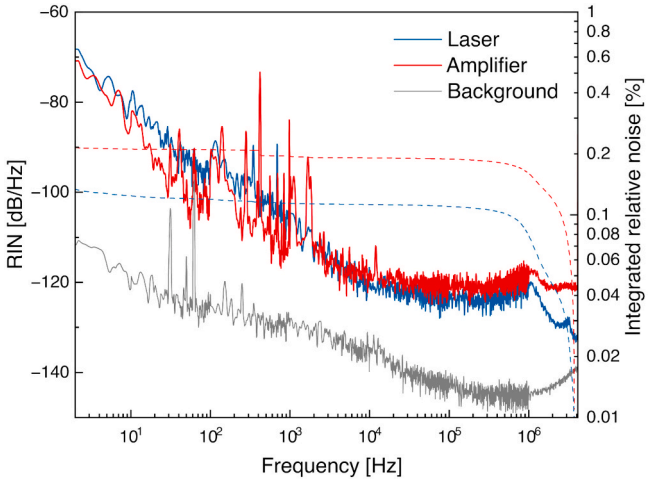

Fig. 8. Left axis: RIN power spectral densities of the MO seeder (blue), the amplifier (red) and the background (grey). Right axis: Integrated relative noise of the MO seeder (blue dashed line) and the amplifier (red dashed line).

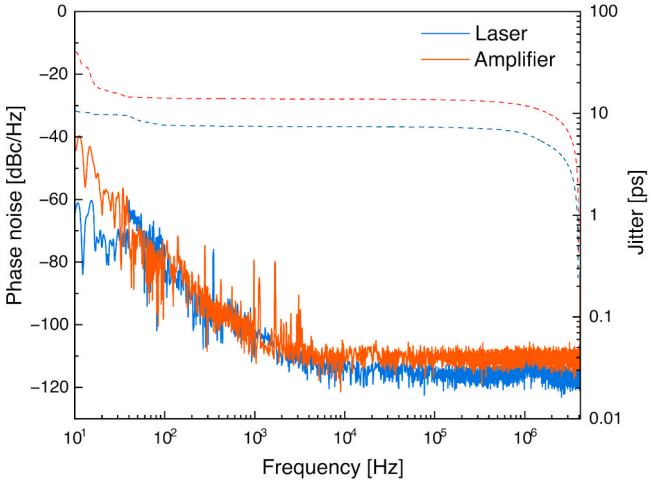

Fig. 9. Left axis: Phase noise two-sided PSD of the MO seeder (light blue) and the amplifier (light red) at the 12th harmonic of the pulse repetition rate (99.6 MHz). Right axis: pulse jitter of the MO (light blue dashed line) and the amplifier (light red dashed line).

For the most effective amplifier configuration, we also carried out a detailed RIN and phase noise characterization of both the MO seeder and the GMNA pulse trains. We measured a very low (~0.2 %) RIN integrated in the range between 2 Hz and 4.15 MHz, which is a direct indication of remarkable system stability. The excellent pulse quality, very high peak power even at a relatively low (~1 W) average power level and very good noise performance, make this robust and compact fiber laser system very promising for nonlinear optics applications such as mid-IR frequency down-conversion or THz generation.

CRediT authorship contribution statement

Sara Pizzurro: Writing – review & editing, Writing – original draft, Validation, Investigation, Formal analysis, Data curation. **Riccardo Gotti:** Writing – review & editing, Supervision, Software, Methodology, Investigation, Formal analysis. **Xhoi Ypi:** Validation, Software, Investigation, Data curation. **Francesco Canella:** Writing – review & editing, Writing – original draft, Validation, Investigation. **Dario Giannotti:** Writing – review & editing, Writing – original draft, Validation, Investigation. **Gianluca Galzerano:** Writing – review & editing, Supervision, Resources, Methodology, Funding acquisition, Formal analysis. **Antonio Agnesi:** Writing – review & editing, Supervision, Methodology, Formal analysis, Conceptualization. **Federico Pirzio:** Writing – review & editing, Supervision, Resources, Project administration, Investigation, Funding acquisition, Data curation, Conceptualization.

Declaration of competing interest

The authors declare that they have no known competing financial interests or personal relationships that could have appeared to influence the work reported in this paper.

Acknowledgments

This work was supported in part by the European Union's NextGenerationEU Programme with the I-PHOQS Infrastructure [IR0000016, ID D2B8D520, CUP B53C22001750006] Integrated infrastructure initiative in PHOtonic and Quantum Sciences; and by ATTILA - Advanced room-Temperature THz hyperspectral Imaging based on novel ultrafast fiber LAsers (20227849RL).

Data availability

The data that support the findings of this study are available from the corresponding author upon reasonable request.

References

[1] M.E. Fermann, I. Hartl, Ultrafast fiber laser technology, IEEE J. Sel. Top. Quantum Electron. 15 (2009) 191–206.
[2] W. Zhao, X. Hu, Y. Wang, Femtosecond-pulse fiber based amplification techniques and their applications, IEEE J. Sel. Top. Quantum Electron. 20 (2014) 512–524.
[3] M.E. Fermann, A. Rolland, The impact of femtosecond fiber lasers in technology and science, Opt. Commun. 574 (2025) 131197.
[4] D. Strickland, G. Mourou, Compression of amplified chirped optical pulses, Opt. Commun. 56 (1985) 219–221.
[5] P. Sidorenko, W. Fu, F. Wise, Nonlinear ultrafast fiber amplifiers beyond the gain-narrowing limit, Optica 6 (2019) 1328–1333.
[6] G. Fu, D. Li, M. Gong, P. Yan, Q. Xiao, Spatiotemporal deterioration in nonlinear ultrafast fiber amplifiers, Appl. Phys. Lett. 123 (2023) 091106.
[7] D. Tomaszewska-Rolla, R. Lindberg, V. Pasiskevicius, F. Laurell, G. Sobon, A comparative study of an Yb-doped fiber gain-managed nonlinear amplifier seeded by femtosecond fiber lasers, Sci. Rep. 12 (2022) 404.
[8] D. Stoliarov, E. Manuylovich, A. Koviarov, D. Galiakhmetova, E. Rafailov, Gain-managed nonlinear amplification of ultra-long modelocked fiber laser, Opt. Express 31 (2023) 43427.
[9] M. Krakowski, G. Soboń, Gain-managed nonlinear amplification in an erbium-doped fiber, Opt. Express 32 (2024) 48815–48823.
[10] H. Ye, L. Pontagnier, E. Cormier, G. Santarelli, Multi-gigahertz femtosecond pulses from linear and nonlinear propagation of a phasemodulated laser, Opt. Lett. 47 (2022) 5405–5408.
[11] E. Poeydebat, G. Santarelli, A. Casanova, F. Scol, O. Vanvincq, G. Bouwmans, E. Hugonnot, Measurements of the absolute timing jitter and intensity noise of an all-fiber Mamyshev oscillator, Opt. Lett. 46 (2021) 2698–2701.
[12] T. Wang, C. Li, B. Ren, K. Guo, J. Wu, J. Leng, P. Zhou, Time jitter and intensity noise of an all-fiber high-power harmonic mamyshev oscillator, J. Lightw. Technol. 41 (2023) 6369.
[13] S. Pizzurro, R. Gotti, L. Carrà, G. Piccinno, A. Agnesi, F. Pirzio, Femtosecond Mamyshev fiber oscillator started by a passively Q-switched microchip laser, Opt. Lett. 47 (2022) 1960–1963.
[14] R. Gotti, S. Pizzurro, F. Canella, D. Giannotti, G. Galzerano, A. Agnesi, F. Pirzio, Femtosecond Mamyshev fiber oscillator started by ultra-low power microchip laser seeder at two different wavelengths: a comparison, Opt. Express 32 (2024) 43635–436433.
[15] E. Treacy, Optical pulse compression with diffraction gratings, IEEE J. Quantum Electron. 5 (1969) 454–458.
[16] P. Sidorenko, F. Wise, Generation of 1 μJ and 40 fs pulses from a large mode area gain-managed nonlinear amplifier, Opt. Lett. 45 (2020) 4084–4087.
[17] J. Zhao, W. Li, C. Wang, Y. Liu, H. Zeng, Pre-chirping management of a self-similar Yb-fiber amplifier towards 80 W average power with sub-40 fs pulse generation, Opt. Express 22 (2014) 32214–32219.
[18] I. Pavlov, E. Dülgergil, E. Ilbey, F.Ö. Ilday, Diffraction-limited, 10-W, 5-ns, 100-kHz, all-fiber laser at 1.55 μm, Opt. Lett. 39 (9) (2014) 2695–2698.